Evaluating SARS-CoV-2 infection under tenofovir-based antiviral prophylaxis: a multi-scale modeling analysis upon experimental data

Pablo M De Salazar[1], Javier Ramos[2], Victor L Cruz[2], Rosa Polo[3], Julia Del Amo[3], Caroline O. Buckee[1], and Javier Martínez-Salazar[2]

[1]Center for Communicable Disease Dynamics, Department of Epidemiology, Harvard School of Public Health, Boston, US.
[2]Byophym group, Institute for the Structure of Matter, Spanish National Research Council (CSIC), Madrid, Spain
[3]National Plan Against AIDS, Ministry of Health, Madrid, Spain

July 6, 2021

Abstract

Tenofovir has shown promising evidence of improving COVID-19 clinical outcomes in observational studies, still to be confirmed in clinical trials. Disease severity might be reduced under prophylaxis with the prodrug tenofovir disoproxil fumarate (TDF), while the protection seems to decrease, or even to lack, when using the alternative prodrug tenofovir alafenamide fumarate (TAF). Aiming to understand why TDF-prophylaxis might reduce COVID-19 severity upon infection we developed a multi-scale analysis framework combining *in vitro* susceptibility data, molecular docking, and within-host dynamics modeling, and using remdesivir–the only antiviral approved to date against COVID-19– as a point of reference.First, our docking model predicted that intracellularly active tenofovir diphosphate binds into the SARS-CoV-2 RNA polymerase in the same site as the antiviral remdesivir triphosphate, but presents lower binding energy, likely reducing the overall inhibition of viral replication and making the antiviral efficacy more susceptible to the drug intracellular concentration. Second, using data from *in vitro* viral cultures with plausible TDF therapeutic concentrations, we estimated that the drug can inhibit SARS-COV-2 replication at an efficacy ranging between 54-99% conditional to the viral cycle length. Third, assuming values approximating this range of inhibition for *in vivo* viral replication during human SARS-COV-2 infection, we found that prophylaxis with TDF with high penetration into viral target cells is capable of delaying viral replication, mitigating direct cell damage and allowing time for the host to mount the adaptive immunity. Last, we found that the potential antiviral effect can be substantially reduced when TDF is given after infection begins. Our work provides a potential mechanistic explanation of the observed clinical effect of TDF against SARS-CoV-2 infection. The proposed inference framework can help to optimize the evaluation of antiviral therapies for COVID-19, in particular those targeting the RNA dependent RNA polymerase.

Introduction

Definitive therapies for treating COVID-19, the disease caused by SARS-CoV-2, are still lacking [1]. Worldwide deployment of potential effective vaccines might still take several months if not years [2] and it remains unknown how they will impact transmission, including SARS-CoV-2 variants of concern. There is still an important need for therapeutic alternatives that help reduce mortality and protect the most vulnerable against infection.

To date, the only antiviral drug recommended for treating COVID-19 is remdesivir [3], although other antivirals are still under research [4]. In addition to remdesivir, tenofovir (as its prodrug tenofovir disoproxil

fumarate, TDF) has shown clinical evidence in preventing COVID-19 morbidity in a retrospective observational study following HIV individuals under antivirals [5], and was associated with reduced mortality in a population cohort in South Africa [6]. Further an association with reduction in infection has been also reported [7]. Remdesivir and tenofovir were originally designed to inhibit the ATP polymerization into the growing nucleic acids chain respectively in a) the Ebola virus polymerase [8]and b) the HIV reverse transcriptase [9]. Remdesivir has been approved for treating COVID-19, based on its efficacy to prevent severe disease and reduce mortality [10]. On the other hand, evidence of the pre-exposure prophylactic efficacy of the nucleotide analogous tenofovir, in particular of TDF in combination with emtricitabine (FTC), has been suggested in an observational study evaluating SARS-CoV-2 infection outcomes among HIV patients under antiretroviral therapy in Spain [5]. Individuals taking TDF/FTC for their HIV infection showed significantly lower risk of SARS-CoV-2 infection and hospitalization compared with individuals taking other antivirals or taking the tenofovir-based prodrug tenofovir alafenamide fumarate (TAF) with FTC. A similar protective trend for TDF/FTC on COVID-19 mortality was observed in South Africa when compared to zidovudine or abacavir-based regimes [11]. Nevertheless, the findings on TDF still need to be confirmed by randomized clinical trials [12], and tenofovir-based therapies are not currently recommended for treating COVID-19. Worth noting, *in vitro* studies have shown contradictory evidence of the potential of TDF to inhibit SARS-CoV-2 replication at plausible therapeutic doses [13,14].

The discrepancy between the different tenofovir prodrugs leading to mixed effectiveness is unexplained yet deserves further analysis. Given the limited resources to screen potential antivirals, and the challenges for implementing clinical trials which are the definitive source of evidence, theoretical modeling can help accelerate drug discovery especially, particularly when coupled with experimental data.

Here, we combined SARS-CoV-2 *in vitro* susceptibility data, molecular docking and within host compartmental modeling, aiming to understand why only prophylaxis with TDF from all tenofovir-based compounds might reduce COVID-19 clinical severity.

Results

Molecular docking

Computed relative binding energies ($\Delta G_{binding}$) showed that remdesivir presented the strongest binding (precision range -8.7 to -8.5 kcal/mol), followed by dATP (-8.6 to -8.4 kcal/mol) and tenofovir (-7.7 to -7.5 kcal/mol). The three ligands shared the same binding site and were forced to adopt a different conformation in order to allow the insertion of the incoming nucleotide into the nascent RNA. Docking structures of dATP, remdesivir, and tenofovir ensembles are displayed in Figure 1. Including the RNA chains/magnesium ions in the analysis reduced the computed $\Delta G_{binding}$ for all three ligands while maintaining a similar affinity gradient (see supplementary material, S2). We further observed that the lowest binding energy conformations did not always show the expected interactions between the template-nascent RNA strands and the analyzed ligand. Thus, we searched for the poses with maximum interaction with the template RNA strand and computed the $\Delta G_{binding}$. In the case of ATP and remdesivir, we found that those poses remain close to the lowest computed $\Delta G_{binding}$ (ca. 0.1 kcal/mol), while the tenofovir ensemble showed a greater difference between the pose with RNA interactions and the lowest $\Delta G_{binding}$ poses (ca. 0.5 kcal/mol). The most probable driver for the lower $\Delta G_{binding}$ of remdesivir compared to ATP is the extra H-bond between the cyano group and the U927 nucleotide of the nascent RNA strand, which is lacking within the tenofovir structure.

In summary, our docking model provides evidence that tenofovir interacts in the same pocket as remdesivir/dATP but presents significantly weaker binding affinity and pose stability, and a relatively stable non-functional binding with the RdRp-CoV2 close to the active pocket.

Estimated inhibition of SARS-CoV-2 replication by TDF

We used data from *in vitro* SARS-CoV-2/Vero-CCL81 cultures in the presence and absence of TDF (3-10 μM to infer the range of inhibition produced by the antiviral to an average single infected cell. Figure 2 shows computed I_{TDF} for viral cycles of length 9.6-48h, which ranged between 0.54 to 0.99 (using the

$2^{-\Delta\Delta Ct}$ approximation) and between 0.50 and 0.98 (using the alternative simple approximation) for the lowest concentration of 3 μM. Experimental Ct and computed VR values using the $2^{-\Delta\Delta\tilde{\tau}}$ approximation are shown in supplementary material Table S2. Given this range of estimates, for the next step we approximated the *in vivo* plausible range of SARS-CoV-2 replication inhibition per cycle due to TDF between 90% (namely high inhibition) and 60% (namely moderate inhibition) approximating the inhibition resulting from a plausible range of 12-36h for the viral cycle [21] .

Within-host model of infection under antiviral treatment

Our simple compartmental model is capable of reproducing the viral dynamics observed during COVID-19 infections, as seen in Figure 3. First, treatment is modeled as prophylaxis: the drug concentrations are at clinical levels when infection begins. Both viral RNA (A) and newly infected cells (B) follow an upward-peak-downward trend. Panel C shows the cumulative number of infected cells. Figure 3 A-C shows that, under full drug penetration (100%), drug inhibition of viral replication mainly leads to a delay in the viral dynamics with almost no impact on the infected cells. For example, moderate efficacy 60% leads to similar viral RNA and infected cells with a ˜ 1 day delay, while high efficacy (90%) leads to a longer delay of ˜ 5 days since infection compared to infection under no treatment; nevertheless, higher efficacy also determines a flatter curve (i.e., widening the distribution of infected cell over time). Also, as seen in panels D-F, dynamics are driven by both penetration and efficacy: very similar patterns are observed under high penetration and moderate efficacy vs. moderate efficacy and high penetration, which is expected given the assumption of homogeneous mixing in the modeled target cell population. Including immune response (panels G-I) shows that a synergistic effect results from an amplified reduction of infected cells due to both treatment and immune control. Interestingly, under innate immunity the cumulative number of infected cells is substantially reduced under prophylaxis and correlated with the efficacy.

Last, we evaluate how time-to-treatment impacts host dynamics. In contrast to the previous assumptions, where drug concentrations are at full efficacious level when viral replication begins, Figure 4 shows how delaying treatment up to 48h (A-C) and 24 h (D-F) before peak viral load reduces the observed delay (to 3 and 0 days respectively, compared to 5 in the main analysis), while the increased distribution of cell infection over times remains similar to earlier treatment.

Discussion

In this work, we show that prophylaxis with tenofovir-based compounds, particularly TDF, might be capable of reducing viral replication during SARS-CoV-2 infection, which in turn might reduce disease severity (and potential mortality). Our findings suggest that this suboptimal clinical effect (i.e. limiting viral growth and subsequent disease severity but not fully blocking viral replication) could arise from suboptimal binding of active tenofovir into the SARS-CoV-2 RNA dependent RNA polymerase. In particular we found in the molecular model that suboptimal tenofovir-RdRp-CoV2 interaction compared to remdesivir, predicting that the ensemble is more sensitive to the phosphate-form intracellular concentration. Thus, matching sufficient intracellular availability of tenofovir-diphostate with SARS-CoV2 tropism [21,26](such as in the respiratory tract [27]) is likely essential in drug-driven containment of viral replication, mirroring what happens during HIV prophylaxis [28]. However, other factors than limited inhibition, including drug-penetration into viral targeted tissues and time-to-treatment relative to exposure are key determinants of infection outcomes.

We used remdesivir as point of reference, which allowed us to validate the predictions of our multi-scale assessment, but also allowed us to explore the underlying process that might lead to limited clinical effect of remdesivir itself against COVID-19. Our findings show that similar intracellular concentrations of remdesivir relative to dATP can effectively inhibit SARS-CoV2 replication, aligned with previous studies [29,30] and experimental evidence [31]. Further, our findings suggest that the limited clinical effectiveness observed for remdesivir [32] might rely on unstudied pharmacokinetic properties and/or time to treatment relative to viral replication rather than drug limited inhibition capacity.

Our docking approach is the first to include template-nascent RNA in the ensemble and further improves previous work [33] by using cryo-EM structures instead of homology and by more extensive sampling of the

ligand poses using volunteer distributed computations. Consistent with our findings, tenofovir-diphosphate has been shown to permanently terminate polymerase extension of nascent RNA when using recombinant RdRp-CoV2 [34]. However, infusion of tenofovir in Vero cell cultures did not inhibit replication of SARS-CoV-2 [13,35], while the use of 3-90 μM of its prodrug TDF yielded a 15-fold reduction of viral genome release as explained before [35] . Further, the use of TDF/FTC for treating SARS-CoV-2 infected ferrets led to better clinical scores and lower virus titers in nasal washes compared to a placebo [36]. Worth noting, the prodrug TDF, formulated to increase tenofovir limited bioavailability [37], is known to diffuse passively across cellular membranes [38,39] and further activate intracellularly, as opposed to tenofovir which requires active transportation for intake before activation [40,41]. Indeed, higher levels of active metabolite after exposure to TDF versus tenofovir has been consistently reported in several cell types [28,42,43]. In contrast, the prodrug TAF was formulated to reduce drug-adverse events observed for TDF (which distributes body-wide) by being highly HIV-target-cell specific. TAF is well known to selectively activate and present preferential distribution in lymphatic tissues [26].

Our overall inference framework is limited by several assumptions at each of the modeling levels. Regarding the molecular docking, while the output is constrained by the common caveats of the approach itself such as the ability of the scoring functions to forecast accurate binding energies, findings from both experimental and previous docking studies are aligned with our findings. As for the *in vitro* estimates, we assumed that the viral dynamics in the experimental environment approximated those *in vivo*; this important caveat can likely only be tested further in clinical studies. However, we used ranged efficacy estimates aiming to produce more flexible scenarios. Further, Zandi et al. [14] reported that TDF did not inhibit SARS-CoV-2 was not inhibited by TDF when using concentrations under 20 microM. Interestingly, in this study Vero cells were not preincubated with TDF in contrast with the procedure from Clososki et al. where cells were preincubated with the drug 24h before virus inoculation, which might explain the discrepancy and aligns with our model predictions.

Our simple within-host modeling approach might not capture important disease mechanisms, such as immune-driven pathogenesis [44]. Further, viral replication can occur in different tissues heterogeneously and at different clinical stages [45], which would lead to more complex dynamics than those represented by our model. Nevertheless, even in the presence of partial immune response, our model shows that the overall antiviral efficacy will ultimately depend on when and where it is available relative to the within-host SARS-CoV-2 distribution.

Together with the existing knowledge on TDF pharmacokinetic/pharmacodynamics, our findings support that TDF, among tenofovir-based compounds, might maximize efficacy at safe clinical dosage especially when taken before or very close after exposure, because of their high cellular permeation, effective metabolite activation, and low-selective distribution at viral targeted tissues, laying out a plausible molecular interpretation of the apparent inconsistency of tenofovir-based compounds against SARS-CoV-2 [46]. Finally, our findings underscore the need for understanding the intracellular availability of the drugs in SARS-CoV2 targeted tissues to further evaluate remdesivir, TDF and other antivirals [12].

In summary, our multi-scale modeling approach provides evidence that the prodrug tenofovir-disoproxil fumarate is a potential candidate to limit disease severity due to SARS-CoV-2 and might maximize its impact when given as prophylaxis; when evaluated in clinical trials, it is expected that its efficacy might depend on the relative time from infection to drug administration as well as for individual PK/PD factors conditioning distribution in SARS-CoV-2 targeted cells. Our work provides a mechanistic explanation of the observed clinical effect of TDF against COVID-19 and can help optimize the evaluation of antiviral therapies for COVID-19, in particular those targeting the RNA dependent RNA polymerase.

Methods

Molecular docking

First, we designed an novel ensemble docking approach derived from crystal structures and implemented with extensive sampling using volunteer distributed computation, 1) to compare the binding location, affin-

ity and stability of the active forms tenofovir-diphosphate (which is comparable to a triphosphate, as tenofovir prodrug already contains one phosphate residue), remdesivir-triphosphate, and deoxyadenosine triphosphate (dATP) with the RdRp-CoV-2- RNA chain complex, 2) to determine the capability of active tenofovir to bind to the RdRp-CoV-2 in order to terminate RNA polymerization, to 3) compare the binding energy and site with that of remdesivir, and 4) to determine potential limitations arising from their molecular structures.

We used the three-dimensional structures of the SARS-CoV-2 RNA-dependent RNA polymerase, solved with RNA nascent and template chains (RdRp-CoV2-RNA, Protein Database Bank entry 7BV1[15]) and the 3 ligands evaluated (dATP, and the biologically active forms of the drugs remdesivir triphosphate [8,16] and tenofovir diphosphate[16]). Ligand structures, along with the type of atoms and the rotatable bonds considered in the docking calculations, are shown in the supplementary material, Section S1 (Figure S1).

Extensive searching in the space of protein-ligand docking conformations was supported by the citizen volunteer computing project COVID-PHYM [17] implemented using the BOINC (Berkeley Open Infrastructure for Network Computing) platform [18]. Around 3.2 million poses were collected for each protein-ligand pair. Further details concerning the analysis of the docked positions are given as supplementary material, Section S2. For comparison with previous approaches, we also performed ensemble docking using the RdRp-CoV2 solved without RNA using the experimental structure deposited in the PDB entry 7BTF [19] (see supplementary material, Section S3).

Estimation of TDF inhibition activity using experimental data from in vitro cultures

Previously, Clososki et al [13] have shown that viral load after 48h *in vitro* Vero CCL81-SARS-CoV2 culture in the presence of TDF leads to a ˜15-fold decrease compared to control culture (i.e. with no antiviral). We aimed to estimate the reduction in viral replication that could be attributed to TDF. Viral load, measured as Cycle threshold (Ct) values obtained from quantitative PCR, were available from monolayers treated with TDF at 3,10,30 and 90 µM (each in triplicate) and monolayers without TDF. We defined the TDF per-cell viral yield inhibition [20] as the average reduction of infected cells arising from one infected cell in the previous cycle, and was computed as the viral replication under 3-10 µM of TDF–assumed to approximate the expected therapeutic range–, relative to the replication in the absence of the antiviral. However, this computation is not straightforward as the exact length of the SARS-CoV-2 viral cycle is not known and might substantially vary [21]. Thus, we aimed to estimate a credible range of the TDF inhibition under the assumption that on average, a complete viral cycle remains between 12h and 36h [20] . First we computed the experimental Viral-load Relative ratio (VR) as the ratio between the $2^{-\Delta\Delta Ct}$ values obtained from each of the TDF-SARS-CoV2 cultures at either 3 or 10 µM divided by the average $2^{-\Delta\Delta\tilde{}\tau}$ of the control cultures (i.e., without antiviral, n=3). Alternatively, the estimation of VR can be roughly computed by assuming that every increase of 3.3 units in the Ct value corresponds with a 10-fold decrease in the viral load [22].

Further, the TDF per-cell viral yield inhibition, I_{TDF} can be computed as proportion 1-Vir_{TDF} /Vir_{null} for each pair of case-control experiment where Vir_{null} is the average number of virions produced per infectious viral particle without the presence of antiviral, and Ver_{TDF} the average number of new virions produced per infectious viral particle in the presence of TDF. The relation between I_{TDF} and VR can be computed for m discrete time steps using the correspondence Vir_{TDF} /Vir_{null} [?] $\sqrt[m]{VR}$. Thus, we estimated the range of I_{TDF} using the experimental VR values (n=12), and m ranging 5 to 1, which simplifies the model approximating a continuous length of the SARS-CoV-2 viral cycle ranging from 9.6 to 48 hours. Details on the derived calculation and experimental data can be found in Supplementary material Section S4.

Within-host model of SARS-CoV-2 infection under antiviral treatment

Last, we implemented a within-host computational model based on ordinary differential equations aiming to evaluate different scenarios regarding treatment efficacy during the first days of the acute infection before adaptive immunity is developed. We formulated a basic frequency-dependent model which allows evaluation of antivirals and has been shown to mimic viral dynamics in the human host for a wide range of viruses [23]. In this model, the viral population is controlled by depletion of target (susceptible) cells. For simplicity the main

model does not assume a significant effect of multiplicity of infection on the viral dynamics [24], nor includes proliferation and death of target cells given the time scale of the analysis. We focus on evaluating the viral population until an efficacious adaptive response is developed, which we assumed to happen around 10 days after infection [25]. Using this model, we evaluated the impact of SARS-CoV-2 infection by estimating the proportion of "tissue" directly damaged by viral infection (as proportion of infected cells from total targeted) while assuming a correlation with disease severity, in the following scenarios: a) infection under preexposure prophylaxis with an antiviral with high inhibition and optimal tissue penetration b) a) infection under preexposure prophylaxis with an antiviral with high inhibition and moderate penetration versus moderate inhibition and high penetration, c) infection under preexposure prophylaxis with an antiviral with high inhibition and existing innate immunity, and d) natural infection and consequent treatment with moderate and high antiviral inhibition and full tissue penetration beginning 24h and 48h before viral load peak. Details on the model formulation and inclusion of immune response can be found in the Supplementary Material Section S5.

References

1. Kim AY, Gandhi RT. Coronavirus disease 2019 (COVID-19): Management in hospitalized adults. [cited 4 Sep 2020]. Available: https://www.uptodate.com/contents/coronavirus-disease-2019-covid-19-management-in-hospitalized-adults

2. Lurie N, Saville M, Hatchett R, Halton J. Developing Covid-19 Vaccines at Pandemic Speed. N Engl J Med. 2020;382: 1969–1973.

3. Beigel JH, Tomashek KM, Dodd LE. Remdesivir for the Treatment of Covid-19 - Preliminary Report. Reply. The New England journal of medicine. 2020. p. 994.

4. Mahase E. Covid-19: UK launches antivirals taskforce to deliver home treatments by autumn. BMJ. 2021;373: n1077.

5. Del Amo J, Polo R, Moreno S, Díaz A, Martínez E, Arribas JR, et al. Incidence and Severity of COVID-19 in HIV-Positive Persons Receiving Antiretroviral Therapy: A Cohort Study. Ann Intern Med. 2020. doi:10.7326/M20-3689

6. Boulle A, Davies MA, Hussey H, Ismail M, Morden E, Vundle Z, et al. Risk factors for COVID-19 death in a population cohort study from the Western Cape Province, South Africa. Clin Infect Dis. 2020 [cited 9 Jun 2021]. doi:10.1093/cid/ciaa1198

7. PREVALENCE AND FACTORS ASSOCIATED WITH SARS-CoV-2 ANTIBODIES IN A SPANISH HIV COHORT. 20 Mar 2021 [cited 9 Jun 2021]. Available: https://www.croiconference.org/abstract/prevalence-and-factors-associated-with-sars-cov-2-antibodies-in-a-spanish-hiv-cohort/

8. Tchesnokov EP, Feng JY, Porter DP, Götte M. Mechanism of Inhibition of Ebola Virus RNA-Dependent RNA Polymerase by Remdesivir. Viruses. 2019;11. doi:10.3390/v11040326

9. Wassner C, Bradley N, Lee Y. A Review and Clinical Understanding of Tenofovir: Tenofovir Disoproxil Fumarate versus Tenofovir Alafenamide. J Int Assoc Provid AIDS Care. 2020;19: 2325958220919231.

10. Wang Y, Zhang D, Du G, Du R, Zhao J, Jin Y, et al. Remdesivir in adults with severe COVID-19: a randomised, double-blind, placebo-controlled, multicentre trial. Lancet. 2020;395: 1569–1578.

11. Davies M-A. HIV and risk of COVID-19 death: a population cohort study from the Western Cape Province, South Africa. doi:10.1101/2020.07.02.20145185

12. Randomized Clinical Trial for the Prevention of SARS-CoV-2 Infection (COVID-19) in Healthcare Personnel - Full Text View - ClinicalTrials.gov. [cited 4 Sep 2020]. Available: https://clinicaltrials.gov/ct2/show/NCT04334928

13. Clososki G, Soldi R, da Silva R, Guaratini T, Lopes J, Pereira P, et al. Tenofovir Disoproxil Fumarate: New Chemical Developments and Encouraging in vitro Biological Results for SARS-CoV-2. Journal of the Brazilian Chemical Society. 2020. doi:10.21577/0103-5053.20200106

14. Zandi K, Amblard F, Musall K, Downs-Bowen J, Kleinbard R, Oo A, et al. Repurposing Nucleoside Analogs for Human Coronaviruses. Antimicrob Agents Chemother. 2020;65. doi:10.1128/AAC.01652-20

15. Yin W, Mao C, Luan X, Shen D-D, Shen Q, Su H, et al. Structural basis for inhibition of the RNA-dependent RNA polymerase from SARS-CoV-2 by remdesivir. Science. 2020;368: 1499–1504.

16. Lou L. Advances in Nucleotide Antiviral Development from Scientific Discovery to Clinical Applications: Tenofovir Disoproxil Fumarate for Hepatitis B. J Clin Transl Hepatol. 2013;1: 33–38.

17. Proyecto COVID-PHYM - Fundación Ibercivis. [cited 8 Sep 2020]. Available: `https://ibercivis.es/project/proyecto-covid-phym/`

18. Anderson DP. BOINC: A System for Public-Resource Computing and Storage. Fifth IEEE/ACM International Workshop on Grid Computing. doi:10.1109/grid.2004.14

19. Gao Y, Yan L, Huang Y, Liu F, Zhao Y, Cao L, et al. Structure of the RNA-dependent RNA polymerase from COVID-19 virus. Science. 2020;368: 779–782.

20. Bar-On YM, Flamholz A, Phillips R, Milo R. SARS-CoV-2 (COVID-19) by the numbers. Elife. 2020;9. doi:10.7554/eLife.57309

21. Chu H, Chan JF-W, Yuen TT-T, Shuai H, Yuan S, Wang Y, et al. Comparative tropism, replication kinetics, and cell damage profiling of SARS-CoV-2 and SARS-CoV with implications for clinical manifestations, transmissibility, and laboratory studies of COVID-19: an observational study. Lancet Microbe. 2020;1: e14–e23.

22. Tom MR, Mina MJ. To Interpret the SARS-CoV-2 Test, Consider the Cycle Threshold Value. Clinical infectious diseases: an official publication of the Infectious Diseases Society of America. 2020. pp. 2252–2254.

23. Perelson AS. Modelling viral and immune system dynamics. Nat Rev Immunol. 2002;2: 28–36.

24. Koelle K, Farrell AP, Brooke CB, Ke R. Within-host infectious disease models accommodating cellular coinfection, with an application to influenza. Virus Evol. 2019;5: vez018.

25. Long Q-X, Liu B-Z, Deng H-J, Wu G-C, Deng K, Chen Y-K, et al. Antibody responses to SARS-CoV-2 in patients with COVID-19. Nat Med. 2020;26: 845–848.

26. Lee WA, He G-X, Eisenberg E, Cihlar T, Swaminathan S, Mulato A, et al. Selective intracellular activation of a novel prodrug of the human immunodeficiency virus reverse transcriptase inhibitor tenofovir leads to preferential distribution and accumulation in lymphatic tissue. Antimicrob Agents Chemother. 2005;49: 1898–1906.

27. Twigg HL, Schnizlein-Bick CT, Weiden M, Valentine F, Wheat J, Day RB, et al. Measurement of antiretroviral drugs in the lungs of HIV-infected patients. HIV Ther. 2010;4: 247–251.

28. Patterson KB, Prince HA, Kraft E, Jenkins AJ, Shaheen NJ, Rooney JF, et al. Penetration of tenofovir and emtricitabine in mucosal tissues: implications for prevention of HIV-1 transmission. Sci Transl Med. 2011;3: 112re4.

29. Shannon A, Le NT-T, Selisko B, Eydoux C, Alvarez K, Guillemot J-C, et al. Remdesivir and SARS-CoV-2: Structural requirements at both nsp12 RdRp and nsp14 Exonuclease active-sites. Antiviral Res. 2020;178: 104793.

30. Pruijssers AJ, George AS, Schäfer A, Leist SR, Gralinksi LE, Dinnon KH 3rd, et al. Remdesivir Inhibits SARS-CoV-2 in Human Lung Cells and Chimeric SARS-CoV Expressing the SARS-CoV-2 RNA Polymerase in Mice. Cell Rep. 2020;32: 107940.

31. Gordon CJ, Tchesnokov EP, Woolner E, Perry JK, Feng JY, Porter DP, et al. Remdesivir is a direct-acting antiviral that inhibits RNA-dependent RNA polymerase from severe acute respiratory syndrome coronavirus 2 with high potency. J Biol Chem. 2020; jbc.RA120.013679.

32. Hsu J. Covid-19: What now for remdesivir? BMJ. 2020. p. m4457. doi:10.1136/bmj.m4457

33. Elfiky AA. Ribavirin, Remdesivir, Sofosbuvir, Galidesivir, and Tenofovir against SARS-CoV-2 RNA dependent RNA polymerase (RdRp): A molecular docking study. Life Sci. 2020;253: 117592.

34. Chien M, Anderson TK, Jockusch S, Tao C, Li X, Kumar S, et al. Nucleotide Analogues as Inhibitors of SARS-CoV-2 Polymerase, a Key Drug Target for COVID-19. J Proteome Res. 2020. doi:10.1021/acs.jproteome.0c00392

35. Liu S, Lien CZ, Selvaraj P, Wang TT. Evaluation of 19 antiviral drugs against SARS-CoV-2 Infection. doi:10.1101/2020.04.29.067983

36. Park S-J, Yu K-M, Kim Y-I, Kim S-M, Kim E-H, Kim S-G, et al. Antiviral Efficacies of FDA-Approved Drugs against SARS-CoV-2 Infection in Ferrets. MBio. 2020;11. doi:10.1128/mBio.01114-20

37. Robbins BL, Srinivas RV, Kim C, Bischofberger N, Fridland A. Anti-human immunodeficiency virus activity and cellular metabolism of a potential prodrug of the acyclic nucleoside phosphonate 9-R-(2-phosphonomethoxypropyl)adenine (PMPA), Bis(isopropyloxymethylcarbonyl)PMPA. Antimicrob Agents Chemother. 1998;42: 612–617.

38. Huttunen KM, Raunio H, Rautio J. Prodrugs–from serendipity to rational design. Pharmacol Rev. 2011;63: 750–771.

39. Arimilli M, Kim C, Dougherty J, Mulato A, Oliyai R, Shaw J, et al. Synthesis, in Vitro Biological Evaluation and Oral Bioavailability of 9-[2-(Phosphonomethoxy)Propyl]Adenine (PMPA) Prodrugs. Antiviral Chemistry and Chemotherapy. 1997. pp. 557–564. doi:10.1177/095632029700800610

40. Kohler JJ, Hosseini SH, Green E, Abuin A, Ludaway T, Russ R, et al. Tenofovir renal proximal tubular toxicity is regulated by OAT1 and MRP4 transporters. Lab Invest. 2011;91: 852–858.

41. Uwai Y, Ida H, Tsuji Y, Katsura T, Inui K-I. Renal transport of adefovir, cidofovir, and tenofovir by SLC22A family members (hOAT1, hOAT3, and hOCT2). Pharm Res. 2007;24: 811–815.

42. Taneva E, Crooker K, Park SH, Su JT, Ott A, Cheshenko N, et al. Differential Mechanisms of Tenofovir and Tenofovir Disoproxil Fumarate Cellular Transport and Implications for Topical Preexposure Prophylaxis. Antimicrob Agents Chemother. 2015;60: 1667–1675.

43. Van Rompay KKA, Babusis D, Abbott Z, Geng Y, Jayashankar K, Johnson JA, et al. Compared to subcutaneous tenofovir, oral tenofovir disoproxyl fumarate administration preferentially concentrates the drug into gut-associated lymphoid cells in simian immunodeficiency virus-infected macaques. Antimicrob Agents Chemother. 2012;56: 4980–4984.

44. Tay MZ, Poh CM, Rénia L, MacAry PA, Ng LFP. The trinity of COVID-19: immunity, inflammation and intervention. Nat Rev Immunol. 2020;20: 363–374.

45. Gallagher ME, Brooke CB, Ke R, Koelle K. Causes and Consequences of Spatial Within-Host Viral Spread. Viruses. 2018;10. doi:10.3390/v10110627

46. Del Amo J, Polo R, Moreno S, Díaz A, Martínez E, Arribas JR, et al. Antiretrovirals and risk of COVID-19 diagnosis and hospitalization in HIV-positive persons. Epidemiology. 2020. doi:10.1097/EDE.0000000000001235

47. Salentin S, Schreiber S, Joachim Haupt V, Adasme MF, Schroeder M. PLIP: fully automated protein–ligand interaction profiler. Nucleic Acids Research. 2015. pp. W443–W447. doi:10.1093/nar/gkv315

48. Amaro RE, Baudry J, Chodera J, Demir Ö, Andrew McCammon J, Miao Y, et al. Ensemble Docking in Drug Discovery. Biophysical Journal. 2018. pp. 2271–2278. doi:10.1016/j.bpj.2018.02.038

49. Evangelista Falcon W, Ellingson SR, Smith JC, Baudry J. Ensemble Docking in Drug Discovery: How Many Protein Configurations from Molecular Dynamics Simulations are Needed To Reproduce Known Ligand Binding? J Phys Chem B. 2019;123: 5189–5195.

50. Morris GM, Huey R, Lindstrom W, Sanner MF, Belew RK, Goodsell DS, et al. AutoDock4 and AutoDockTools4: Automated docking with selective receptor flexibility. J Comput Chem. 2009;30: 2785–2791.

51. Livak KJ, Schmittgen TD. Analysis of relative gene expression data using real-time quantitative PCR and the 2(-Delta Delta C(T)) Method. Methods. 2001;25: 402–408.

52. Abernathy E, Glaunsinger B. Emerging roles for RNA degradation in viral replication and antiviral defense. Virology. 2015;479-480: 600–608.

53. Sungnak W, Huang N, Bécavin C, Berg M, Queen R, Litvinukova M, et al. SARS-CoV-2 entry factors are highly expressed in nasal epithelial cells together with innate immune genes. Nat Med. 2020;26: 681–687.

Data availability: Experimental data from SARS-CoV-2 viral cultures used in this analysis is provided in the Supplementary Material. Code and ligand-receptors structures used in the molecular docking are available from the authors upon request. Codes for the within host model are publicly available at github.com/pdesalazar.

Conflicts of interest: There are no conflicts to declare.

Author's contribution: PMD, JR, JMS, CB, JDA and RP conceived the idea. PMD, JR, and JMS designed the ensemble docking model. JR and VLC performed the docking computations. PMD designed and analysed the statistical models for in vitro and within host dynamics under the supervision of CB. PMD, JR, JMS and CB wrote the manuscript with support of VLC, RP and JDA.

Acknowledgements: We thank the authors of [13] for providing access to the *in vitro* culture data. We thank Francisco Sanz García and Daniel Lisbona of the Ibercivis Foundation for their assistance in the use of the BOINC platform. We also thank Miguel Hernán and Jose Ramón Arribas for their technical advice. Finally, we acknowledge the volunteers who contributed to the COVID-PHYM project using BOINC distributed computing networks.

Funding: JR was supported by the CSIC (PIE202050E017) for financial support. PMD. was partly supported by the Ramon Areces Foundation, postdoctoral grant. PMD and COB were supported by the Burroughs Wellcome Fund.

Figures

Figure 1 Analysis of the interactions between the ATP, remdesivir, and tenofovir ligands with the RdRp receptor containing template-nascent RNA and Mg ions.

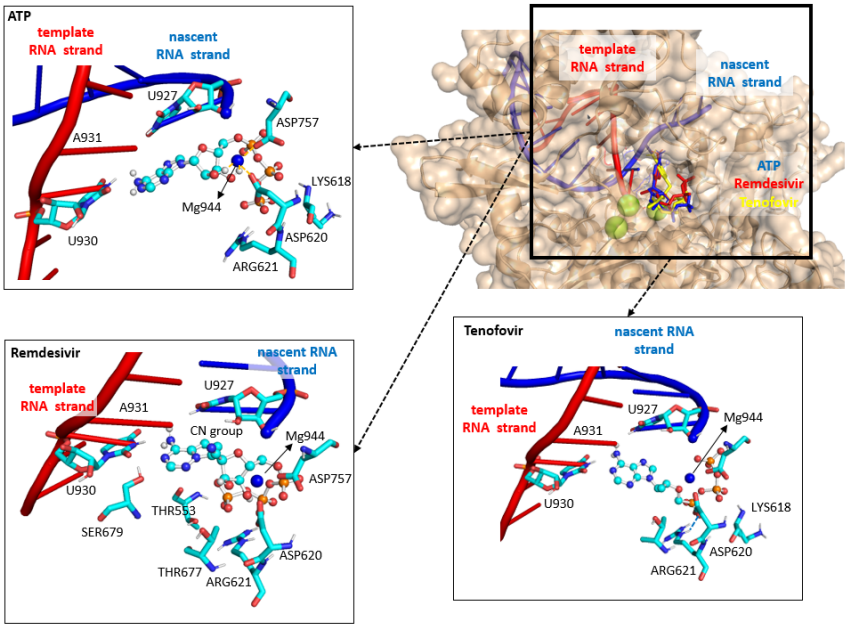

Figure 1: This is a caption

Figure 1: Ligands are displayed as ball-and-stick; RNA and amino acid residues interacting with the ligands are shown as sticks; and magnesium ions are shown as a blue Van der Waals sphere. The square represents the approximate grid box used to perform the docking studies. The analysis of the interactions was carried out using the Protein-Ligand interaction profiler (PLIP)[47] and Discovery Studio. Images were prepared using Pymol 2.4.0.

Figure 2. Range estimates of in vitro SARS-CoV-2 replication inhibition by TDF (at 3 and 10 microM) relative to plausible viral cycle lengths

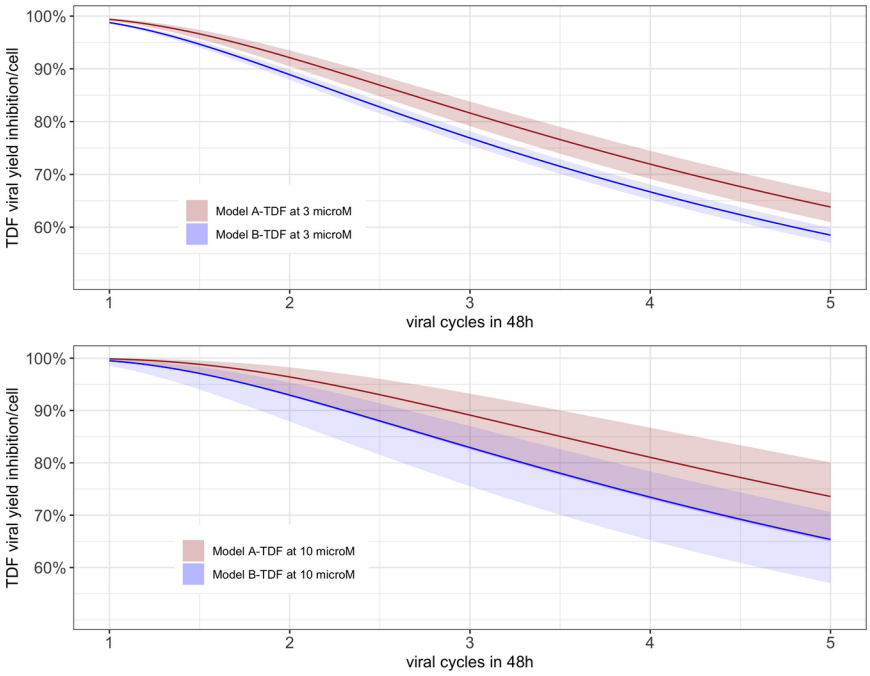

Figure 2: This is a caption

Figure 2. Showing per cell TDF inhibition viral yield for m =1 to 5 (viral cycle length ranging 48h to 9.6h) at 3 microM (top panel) and 10 microM (bottom panel). Solid and dashed lines represent mean values computed using the two different models (the $2^{-\Delta\Delta Ct}$,namely Model A in red, and the simplest model assuming each Ct˜ 3.3, namely model B, in blue), and ribbon represents the uncertainty around the mean based on standard errors.

Figure 3. Modeled estimates (normalized) of viral population and infected cells dynamics over time (as newly infected cells and as cumulative proportion of cells per time step) under TDF-prophylaxis with different drug efficacy, drug penetration and innate immunity scenarios.

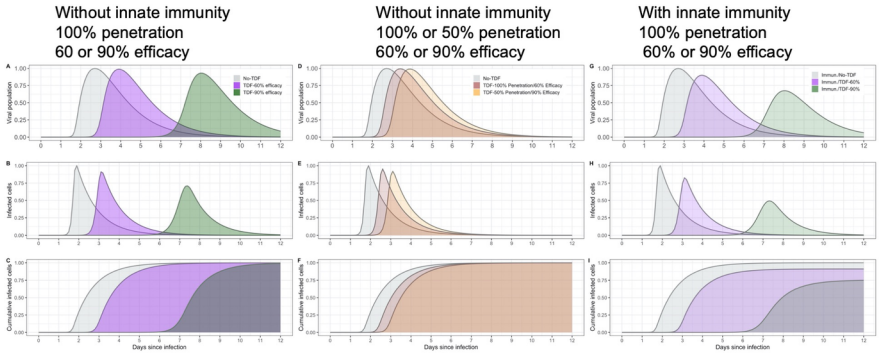

Figure 3: This is a caption

Figure 3 Showing viral dynamics (A,D, G) and infected cells,(B,E,H representing newly infected cells; and C,F,I represent the cumulative infected proportions as a proxy of tissue damage over time). In A-

C penetration of the target cells is assumed to be optimal. Grey represents infection without antivirals, purple represents infection under moderately effective antiviral (60% inhibition) and green represents highly effective antiviral (90% inhibition). In D-F, penetration and/or inhibition are suboptimal: light orange represents 50% penetrance coupled with 90% inhibition and light brown represents 100% penetration with 60% inhibition. In G-I, the model includes basic innate immunity activated by infected cells density. Again, grey represents infection without antivirals, purple represents infection under moderately effective antiviral (60% inhibition) and green represents highly effective antiviral (90% inhibition).

Figure 4. Estimates of viral population and infected cells dynamics under RT-type antiviral treatment with time-of-treatment closer to viral peak and without innate immunity.

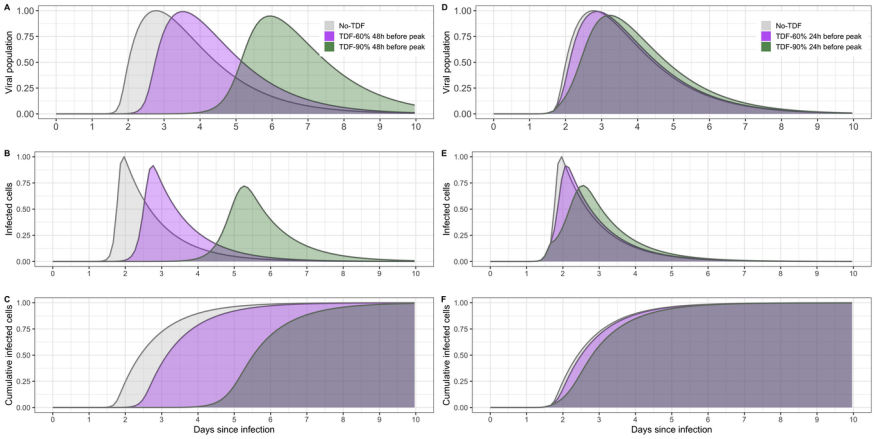

Figure 4: This is a caption

Figure 4 Viral dynamics and infected cells (tissue damage) under TDF-like antiviral treatment without innate immunity. A-C treatment with TDF-like antiviral starting 48h before expected peak viral load and D-F starting 24h before expected peak viral load. Grey represents infection without antivirals, purple infection under moderately effective antiviral (60% inhibition) and green highly effective antiviral (90% inhibition).